J Appl Physiol 121: 233–247, 2016.
First published May 19, 2016; doi:10.1152/japplphysiol.00715.2015.

Static and dynamic stress heterogeneity in a multiscale model of the asthmatic airway wall

J. E. Hiorns,[1] O. E. Jensen,[2] and B. S. Brook[1]

[1]*School of Mathematical Sciences, University of Nottingham, Nottingham, United Kingdom; and* [2]*School of Mathematics, University of Manchester, Manchester, United Kingdom*

Submitted 24 August 2015; accepted in final form 15 May 2016

Hiorns JE, Jensen OE, Brook BS. Static and dynamic stress heterogeneity in a multiscale model of the asthmatic airway wall. *J Appl Physiol* 121: 233–247, 2016. First published May 19, 2016; doi:10.1152/japplphysiol.00715.2015.—Airway hyperresponsiveness (AHR) is a key characteristic of asthma that remains poorly understood. Tidal breathing and deep inspiration ordinarily cause rapid relaxation of airway smooth muscle (ASM) (as demonstrated via application of length fluctuations to tissue strips) and are therefore implicated in modulation of AHR, but in some cases (such as application of transmural pressure oscillations to isolated intact airways) this mechanism fails. Here we use a multiscale biomechanical model for intact airways that incorporates strain stiffening due to collagen recruitment and dynamic force generation by ASM cells to show that the geometry of the airway, together with interplay between dynamic active and passive forces, gives rise to large stress and compliance heterogeneities across the airway wall that are absent in tissue strips. We show further that these stress heterogeneities result in auxotonic loading conditions that are currently not replicated in tissue-strip experiments; stresses in the strip are similar to hoop stress only at the outer airway wall and are under- or overestimates of stresses at the lumen. Taken together these results suggest that a previously underappreciated factor, stress heterogeneities within the airway wall and consequent ASM cellular response to this micromechanical environment, could contribute to AHR and should be explored further both theoretically and experimentally.

airway hyperresponsiveness; circumferential stress; extracellular matrix; tidal breathing; deep inspirations

NEW & NOTEWORTHY

Airway geometry, and the interplay between dynamic active and passive forces, give rise to large stress and compliance heterogeneities across the broncho-constricted intact airway wall that are absent in tissue strips with identical properties. These findings suggest a redesign of loading protocols in tissue-strip experiments to better mimic the dramatically different micromechanical conditions experienced by airway smooth muscle cells in the intact airway. Consequent cellular response could play an important role in airway hyperresponsiveness.

DESPITE SIGNIFICANT RESEARCH effort, mechanisms underlying hyperresponsiveness (AHR) of airway smooth muscle (ASM) and consequent airway narrowing, a key characteristic of asthma, remain poorly understood. Factors that may modulate AHR in the presence of contractile agonist have been investigated experimentally through a variety of assays ranging from stretch experiments on ASM tissue strips (3, 6, 34) and precision cut lung slices (23) to applications of pressure and volume fluctuations on isolated intact airways (9, 21, 28). The tissue-strip assay, in particular, has been used extensively in numerous studies [e.g., most recently by Lan et al. (20)] aimed at investigating AHR. Observations between the different experiments have sometimes been difficult to reconcile given the potentially different strains being imposed, the existence (or lack) of parenchymal tethering, and changes in geometry such as between the strip and the intact airway. Here, we hypothesize that the geometry and structure of the intact airway wall in vivo and in vitro potentially provide a dynamic micromechanical environment to the ASM not present in the isolated ASM strip, which may in turn play an important role in AHR.

To understand the influence of these different factors in both quasistatic and dynamic conditions, an ideal experiment would be one in which results from applying transmural pressure fluctuations to an intact airway could be compared directly with results from applying length or force fluctuations to a strip of ASM isolated from the same airway. Ideally also, identical loading conditions would be applied in both cases, with equivalent measures of contraction being recorded. Given the difficulty of such a proposition, in this study we use a multiscale airway model developed previously (10), which significantly extends earlier models of airways embedded in parenchyma (17, 19, 22, 26, 33, 30) to effectively conduct such an experiment in silico (Fig. 1). This model assumes an intact thick-walled airway embedded in parenchyma and accounts for *1*) nonlinear elasticity of the airway wall (allowing for large deformations); *2*) extracellular matrix (ECM) through the addition of helical collagen fibers (recruited on inflation) within the airway wall; and *3*) dynamic force-generation through subcellular acto-myosin interactions modelled explicitly using the Huxley-Hai-Murphy model. Using this model we have previously illustrated the effect of applying contractile agonist on airway narrowing at different transmural pressures and how the quasistatic pressure-radius relationships of isolated intact airways are modified accordingly. Furthermore we demonstrated that application of fixed-amplitude transmural pressure (P_{TM}) fluctuations at a fixed mean P_{TM} is able to reduce mean contractile force at the cell level within the airway, but the integrative response (which incorporates strain stiffening through collagen recruitment) of the whole airway to the pressure fluctuations was typically of only a small increase in airway caliber relative to the static case (in agreement with experiment; Ref. 21). However, the same amplitude of P_{TM} fluctuations could promote significant bronchodilation at transmural pressures in the most compliant part of the quasistatic P_{TM}-radius curve. These predictions have been confirmed experimentally by Harvey et al. (9), who tested the effect of applying increasing amplitude P_{TM} fluctuations at two values of simulated functional residual capacity (1 and 5 cmH_2O).

Address for reprint requests and other correspondence: B. S. Brook, School of Mathematical Sciences, Univ. Park, Univ. of Nottingham, Nottingham, NG7 2RD, UK (e-mail: bindi.brook@nottingham.ac.uk).

  ISSN 8750-7587.

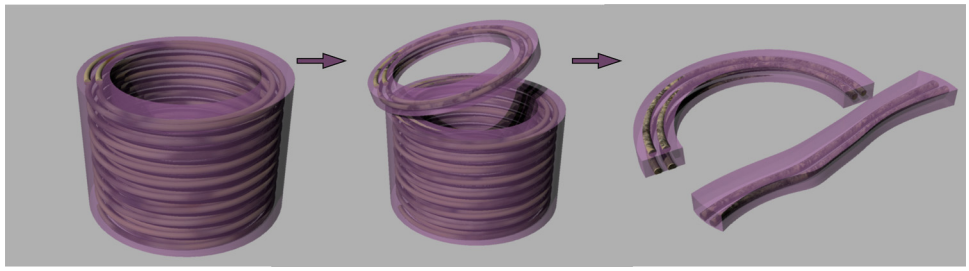

Fig. 1. Schematic of the circular airway smooth muscle (ASM) and collagen fibers embedded within the intact isolated airway wall and the virtual tissue strip as though cut from the original airway. In reality the strips can be as long as depicted; e.g., typical dimensions from Lan et al. (20) are 1- to 1.5-mm wide, 0.2- to 0.3-mm thick, and ~6 mm in length from a sheep trachea that has a diameter ~25 mm.

They found significantly higher strains and bronchodilation at 1 cmH_2O, supportive of the hypothesis that greater bronchodilation of the airway is possible in the more compliant region of the P_{TM} -radius curve.

The purpose of the present study is twofold. First, we wish to explore the consequences of contractile force generation together with quasistatic and dynamic pressure fluctuations on the internal stresses in the airway wall and therefore the difference in the static vs. dynamic microenvironment to which ASM is subjected within the airway wall. To date, this has not been possible in airway models in which the Laplace approximation for thin-walled cylinders has been assumed, or relatively simple force-velocity or force-length relationships have been prescribed. Secondly we wish to investigate the effect of applying identical strains to both an intact airway and a tissue strip on the stresses experienced by ASM. To achieve this, we develop a model for the tissue strip with the appropriately modified geometry (i.e., that of a narrow strip "cut" from a circumferential segment of the virtual airway; Fig. 1) where we apply the same material properties and modeling assumptions as we did for the airway wall (10). We mimic the application of both quasistatic pressure changes and time-dependent P_{TM} fluctuations to the airway model to fully explore and quantify the resulting circumferential strains and circumferential (hoop) stresses within the airway wall (Fig. 2). We then apply the circumferential strain predictions from the airway model to the tissue strip as longitudinal time-dependent length fluctuations. These result in longitudinal stresses in the strip that can then be directly compared with circumferential stresses within the airway wall. We are thus able to carry out a systematic comparison between intact airways and tissue strips to specifically investigate the effect of *1*) geometry (circular airway vs. long thin rectangular strip) and *2*) modification of smooth muscle to collagen content (as may occur in preparation of strips in experiment).

METHODS

In this section we briefly describe two mathematical models, one for an intact airway and the other for a tissue strip and outline the simulations that enable us to compare the two cases. Full details for

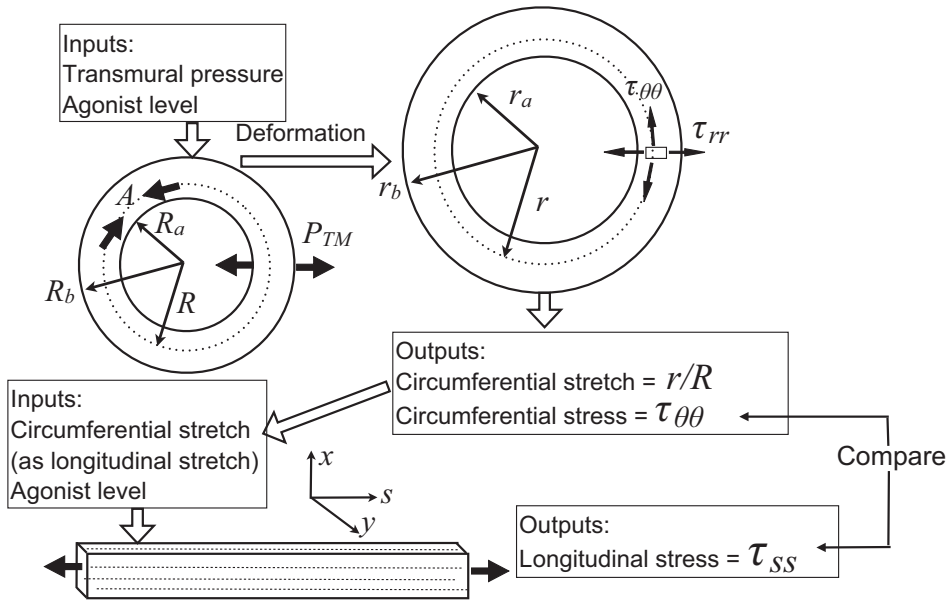

Fig. 2. The airway is assumed to be an axisymmetric cylinder of fixed length. R_a and R_b are the undeformed radii of the inner wall of the airway (lumen) and outer wall of the airway, respectively. r_a And r_b are the corresponding deformed radii. Rings of ASM and collagen fibers are embedded into the airway with representative fibers shown as dashed lines located at a general radius R and r in the undeformed and deformed states respectively. There are many such fibers, represented in the model as a density. The active contractile force, A, produced within the fibers is governed by the Huxley-Hai-Murphy model developed by Mijailovich et al. (27), which combines the Huxley sliding theory (15) and the Hai-Murphy four-state theory (8) (see Ref. 10 for details). The tissue strip is assumed to be long and thin. Fibers are embedded in the strip along the s-axis (shown by dashed lines). Material parameters are the same as in the airway wall. Application of transmural pressure fluctuations and agonist in the model gives predictions of time-dependent circumferential strains and stresses within the airway. The dynamic circumferential strain at the undeformed midpoint of the wall $(R_b - R_a)/2$ is applied to the tissue strip as a length fluctuation which results in the generation of dynamic longitudinal stress. The predicted circumferential (hoop) stress and longitudinal stresses are compared with each other.

the airway model are provided in Hiorns et al. (10) and details for the tissue strip model are provided in the APPENDIX.

Intact Airway Model

We model an airway as an axisymmetric thick-walled cylinder of fixed length in a plane-strain approximation (with no axial displacement). We assume that the airway wall is an incompressible nonlinear elastic material embedded with fibers representing ASM and collagen that form rings in the airway wall (Fig. 1). The fibers combine both passive and active functions: they stiffen during inflation (above a threshold strain) to mimic recruitment of collagen within the ECM and they generate a contractile force upon ASM activation. The passive features contribute stiffness to an inflated airway, for which an exponential increase in energy in the fibers is required to stretch the fibers further. Two parameters, C_1 and C_2, govern the stiffness of the fibers: C_1 takes into account the density of fibers (assumed to be uniformly distributed across the airway wall) and their stiffness when stretched a small amount; C_2 governs the nonlinear increase in the stiffness of the fibers as they stretch. The magnitude of the contractile force, generated through application of agonist, is determined via the Huxley-Hai-Murphy (HHM) model (27), which yields the number and stretch of attached cross bridges and hence the force generated by a single contractile unit (consisting of a myosin filament and adjacent actin filaments). To calculate the contractile force per unit cross-sectional area of tissue, A, we multiply the force generated by a contractile unit (i.e., an actin-myosin filament pair) by a parameter β, which takes into account the volume fraction of the ASM fibers and the number of parallel myosin filaments within a single ASM fiber (10). To couple the velocity of the contractile unit to that of the tissue, we relate the length of the fiber to that of a contractile unit as described in Hiorns et al. (10). We assume that the airway is isolated from the parenchyma and that initially an internal stress is applied to the airway to partially inflate it (as done experimentally). To mimic pressure fluctuations applied experimentally, a time-dependent force is applied at the inner boundary of the airway.

Upon activation via agonist or on application of a transmural pressure, airway wall deformation is characterized by changes in the undeformed inner and outer wall radii (R_a and R_b respectively; Fig. 2) to deformed inner and outer airway wall radii (r_a and r_b, respectively, which may be functions of time; Fig. 2). Resulting stresses in the radial, hoop, and axial directions are written as τ_{rr}, $\tau_{\theta\theta}$, and τ_{zz}, respectively; the radial stress at the lumen boundary is τ_a and the radial stress at the outer boundary is τ_b. Coupling of the subcellular HHM model to the nonlinear elasticity model of the airway enables prediction of dynamic changes in contractile force, radial, and hoop stresses and airway wall deformations.

Tissue Strip Model

We model the tissue strip as a long thin strip of nonlinear elastic material embedded with ASM and collagen fibers oriented longitudinally (full details are given in the APPENDIX), under the assumption that a strip is cut perpendicular to the longitudinal axis of the airway (Fig. 1, *right*, and 2). To carry out the in silico experiment suggested in Fig. 1 we assume identical material properties and fiber stiffness and density parameters as the airway wall. We neglect the intrinsic curvature of an excised slice that may exist by assuming that the strip has a stress-free state in which it is straight. Length fluctuations are applied to the model of the tissue strip, and the corresponding contractile force generated by the ASM and resultant stresses are predicted. We also investigate variations in the density of ECM and ASM by varying the parameter C_1 associated with fiber stiffness. The only nonzero stress is in the axial (s-) direction, τ_{ss} (Fig. 2). Ignoring boundary effects, τ_{ss} is spatially independent, depending only on the stretch of the strip and the amount of agonist (see APPENDIX). This is in contrast to τ_{rr} and $\tau_{\theta\theta}$ above, which depend on radial position.

RESULTS

We have previously established the validity of our airway model (10) by comparing simulation predictions (of the effect of transmural pressure oscillations on lumen radius) with experimental data from LaPrad et al. (21). Here we focus on the effect of quasistatic changes and dynamic oscillations in transmural pressure on hoop stresses within the airway wall and compare these to longitudinal stresses predicted via tissue strip simulations. We then explore the effect of modifications to smooth muscle content on hoop stresses within the wall and again consider how these compare to longitudinal stresses in the tissue strip.

The simulations are based on the two experimental protocols of LaPrad et al. (21). In each protocol, the airway begins in a prestressed state, in which agonist concentration is zero and some initial transmural pressure (P_{TM0}) is applied. The subsequent protocols are as follows.

Protocol 1: increasing levels of agonist concentration are applied to the airway (each period is 12 min) during *1*) static conditions and *2*) application of transmural pressure oscillations of fixed amplitude to mimic tidal breathing.

Protocol 2: initially agonist is applied to the airway so that it contracts for 15 min. Transmural pressure oscillations of increasing amplitude (each for 15 min) are then applied to the constricted airway while agonist concentration is held fixed.

In these simulations, the contractile force generated through application of increasing agonist concentration is mimicked by varying the myosin light chain kinase rate constant (k_1) in the HHM model. The application of a transmural pressure difference, P_{TM}, is achieved by prescribing

$$P_{TM} = P_{TM0} + \Delta P_{TM} \sin\left(\frac{2\pi t}{t_0}\right), \qquad (1)$$

where ΔP_{TM} is the amplitude of the transmural pressure oscillations. Here the period of oscillation $t_0 = 5$ s matches the experiments of LaPrad et al. (21). Table 1 gives the parameter values used for each protocol. The transmural pressure is generated by setting the stress at the outer boundary, τ_b, to zero and varying the stress acting on the lumen, τ_a, in the time-dependent manner described by (*Eq. 1*) with $\tau_a = P_{TM}$. These boundary conditions are chosen specifically to match experimental conditions; the appropriate boundary condition for simulating an in vivo case would be to vary τ_b and fix τ_a, mimicking the effect of the pleural pressure pulling the airway outward. For the airways used in the experiments of LaPrad et al. (21), under zero transmural pressure, the undeformed thickness is ~0.3 times the lumen radius ($R_b = 1.3R_a$).

Table 1. *Table of the parameters used in the airway for the 2 protocols*

Case	P_{TM0}	ΔP_{TM}	$k_1(s^{-1})$	χ	β	g_1, s^{-1}
Protocol 1	7.5	0, 2.5	0.005, 0.025, 0.05	$0.3R_a$	100	0.1
Protocol 2	5	0, 1.25, 2.5, 5	0.025	$0.3R_a$	100	0.1, 0.01

Pressures are measured in cmH_2O. P_{TM}, transmural pressure; χ, wall thickness in terms of the lumen radius when zero transmural pressure is applied; k_1, phosphorylation rate of myosin cross bridges via myosin light chain kinase [in the Huxley-Hai-Murphy (HHM) model] and proportional to agonist level in our simulations; g_1, parameter that governs the strain-dependent detachment of so-called latch bridges (in the HHM model); remaining rate parameters used are as given in Mijailovich et al. (27).

Effect of Transmural Pressure Oscillations on Hoop Stress and Regional Compliance

Although the lumen radius, airway wall thickness and strain can be measured experimentally in isolated intact airways (9, 21) and in precision-cut lung slices (33, 23), ASM and transmural pressures generate hoop (or circumferential) and radial stresses in the airway wall that are not currently amenable to observation. These are important quantities for understanding the tissue microenvironment and for direct comparison with tissue strip experiments, as the hoop stress is the most equivalent to the longitudinal force generated in tissue strips; the tension in the strip is proportional to the longitudinal stress along it. The stress heterogeneity across the airway wall predicted by Brook et al. (4) is also predicted by the present model for static transmural pressure (Fig. 3*A*) applied to an activated airway. At $P_{TM} = 7.5$ cmH_2O, the static hoop stress, $\tau_{\theta\theta}$, at the inner wall decreases with increasing agonist (and can become compressive; see later) while it remains tensile at the outer wall (Fig. 3*A*). The compressive hoop stress can be explained by considering the forces acting on a tissue element within the airway wall (Fig. 3*B*). Close to the lumen, the active component of the hoop stress, pulling the faces of the element inwards, can be smaller in magnitude than the passive component of the element pushing outwards (like an internal spring in compression). Closer to the outer wall, the active component of the hoop stress is greater than the passive component, generating a tensile force.

These stress distributions are modified by the applied transmural pressure (via the radial stresses τ_{rr}; Fig. 3*B*) and the level of activation of smooth muscle as illustrated in Fig. 4. This figure shows static hoop stress-radius curves (black curves) for increasing agonist. Superimposed on these are static transmural pressure isolines (red and blue curves) indicating how application of a given static P_{TM} results in a particular radius and hoop stress. To highlight the effect of the stress heterogeneity, stress-radius curves are shown for hoop stress at the outer radius (Fig. 4*A*) as well as at the lumen radius (Fig. 4*B*). We also superimpose on these the dynamic stress-radius loops that result from P_{TM} oscillations for *protocol 1* (green loops) and *protocol 2* (magenta loops). We observe the following strikingly contrasting behavior between the outer wall and inner wall.

For $P_{TM} \leq 0$ and increasing agonist, static hoop stress increases at the outer wall but decreases at the lumen. The static outer hoop stress and undeformed outer radius for a nonactivated airway are given by the intersection of the zero-agonist curve and the zero P_{TM} curve (Fig. 4*A*). Increasing agonist while keeping $P_{TM} = 0$ causes an increase in hoop stress at the outer wall as the airway narrows. This is as would be expected, given that contractile force increases with increasing agonist. This is also true for negative transmural pressure as indicated by the light blue curves for $P_{TM} < 0$. At the lumen, however, the hoop stress decreases with increasing agonist (as is so for all P_{TM}). We return to this point in the DISCUSSION.

For a range of positive transmural pressures, agonist-induced contraction can reduce hoop stress at the outer wall by derecruitment of collagen fibers. In contrast to previous theoretical predictions (22) (reproduced below, see Fig. 8) in which hoop stress always increases for increasing contraction, for a range of transmural pressures (red curves in Fig. 4*A*) we find

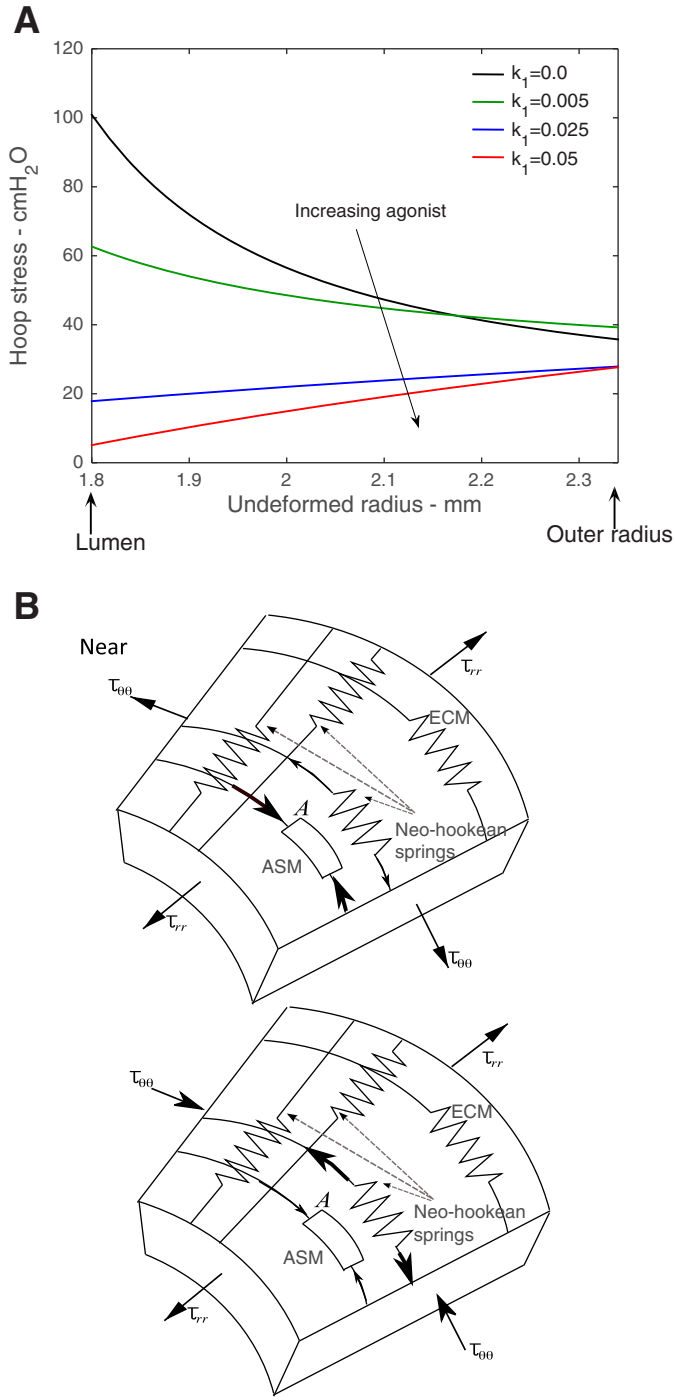

Fig. 3. *A*: static hoop stress plotted as a function of position within the airway wall at $P_{TM} = 7.5$ cmH_2O for increasing agonist, with the black curve representing hoop stress distribution at zero agonist and the red curve the highest agonist level $k_1 = 0.05$, used in *protocol 1* simulations. *B*: schematic illustrating the magnitude of the active force, *A* (width of the arrows indicate magnitude), relative to the passive forces within a tissue element near the lumen and the outer wall. Near the lumen, the active force can be smaller than the passive force and so the resulting hoop stress on neighboring elements can be compressive (i.e., $\tau_{\theta\theta} < 0$) while at the outer wall the active force can be much greater generating a tensile hoop stress ($\tau_{\theta\theta} > 0$). ECM contributes to the passive forces as it is recruited during stretch but not during shortening when it becomes derecruited.

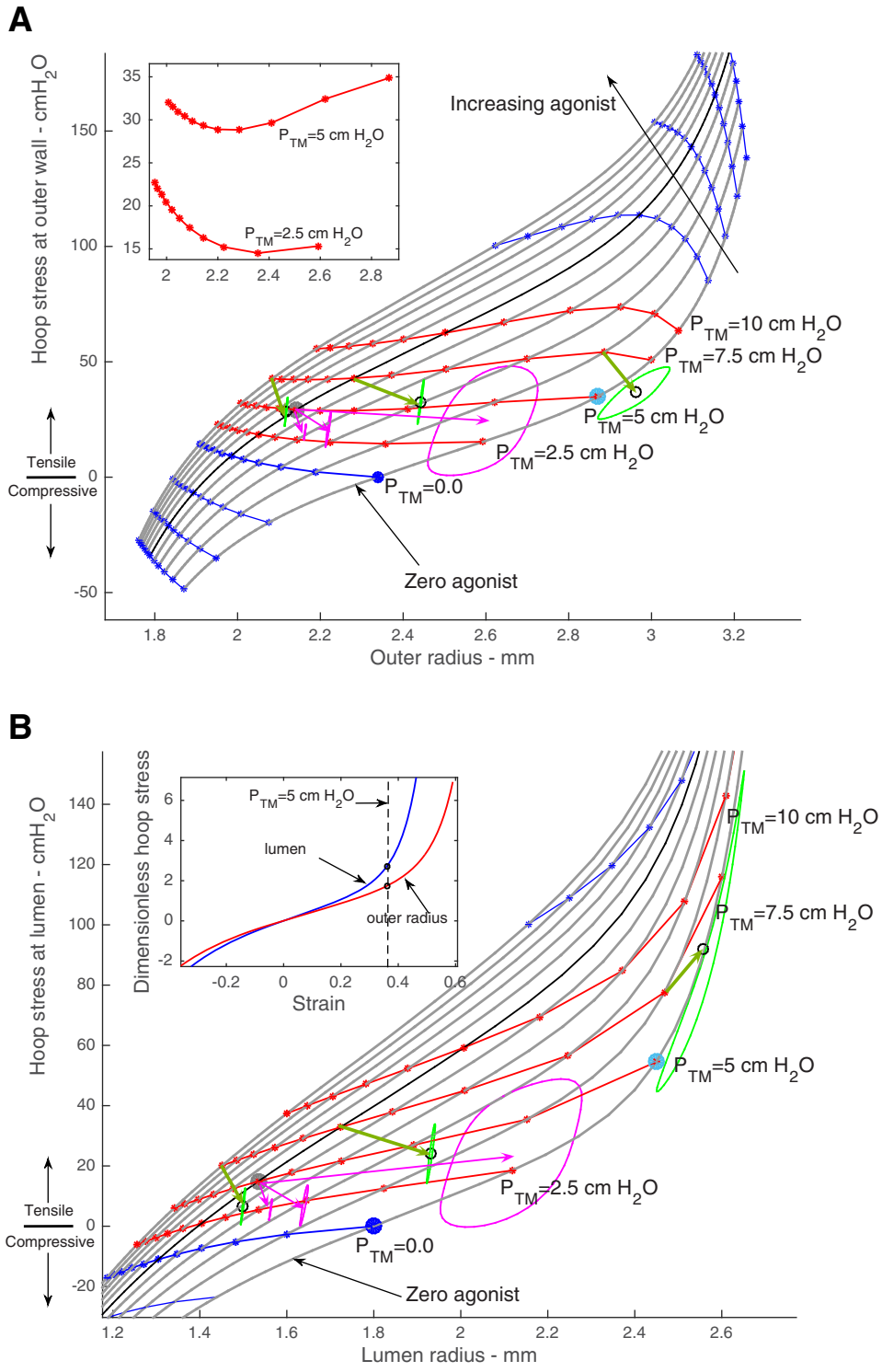

Fig. 4. Static hoop stress at the outer wall plotted as a function of the outer radius (*A*) and static hoop stress at the lumen plotted as a function of lumen radius for increasing agonist (*B*) (black curves; $k_1 = 0$ up to $k_1 = 0.05$). Points on the black curves that are of equal transmural pressure are connected by the red and blue curves and are effectively transmural pressure isolines. Green hoop-stress/radius loops are results of the *protocol 1* simulations showing the effect of increasing agonist on transmural pressure oscillations of fixed amplitude with $P_{TM0} = 7.5$ cmH_2O. Magenta hoop-stress/radius loops are results of *protocol 2* simulations in which increasing amplitude pressure oscillations are applied about $P_{TM0} = 5$ cmH_2O at a fixed agonist level. The dark blue solid circle refers to the unactivated, unstressed state, the cyan solid circle refers to the baseline, initially pre-stressed, state [axis label *B* in Fig. 7, *B* and *C*) and the gray solid circle refers to the contracted state (i.e., after application of agonist; axis label *C* in Fig. 7, *B* and *C*) for *protocol 2* simulations. Short green arrows indicate the shift from the static hoop stress and radius at P_{TM0} to the mean hoop stress and radius of each green loop for *protocol 1* simulations indicated by the black open circles. Magenta arrows indicate the shift from the grey solid circle for the *protocol 2* simulations. *A*, inset: a zoom-in of the isopressure curves for $P_{TM0} = 2.5$ and 5 cmH_2O showing modification in hoop stress-radius behavior. *B*, *inset*: dimensionless hoop-stress at lumen and outer wall as functions of strain overlaid on each other to illustrate different stress-strain behavior at the 2 airway locations.

that hoop stress decreases to a minimum with increasing agonist before increasing again (Fig. 4*A*, *inset*). This can be explained by considering the following events. Application of a positive transmural pressure with no agonist causes distension of the airway (moving up the zero agonist curve) above the threshold at which collagen is recruited. This causes the passive component of the hoop stress to increase as a result of nonlinear strain stiffening. Application of agonist from this point, while keeping transmural pressure fixed, causes the airway to contract, reducing the outer wall radius (Fig. 4*A*, red curves and *inset*), in the process derecruiting collagen fibers and leading to an initial decrease in hoop stress. The decrease in the magnitude of the passive component is thus greater than the increase in the active component due to increased agonist. At radii below the collagen recruitment threshold, agonist-driven increase in the active force dominates and ensuing

behavior is as expected (i.e., hoop stress now increases with further increase in agonist).

The quasistatic mechanical behavior of the airway is significantly modified in the dynamic regime. Protocol 1 oscillations are applied at a mean of 7.5 cmH_2O, but the mean values of the outer hoop stress and outer radii (open black circles in Fig. 4*A*) of each of the stable oscillatory solutions (green loops) now follow a different pressure isoline that appears to have shifted downwards and closer to the static 5 cmH_2O curve. In each *protocol 1* case, therefore, there is a reduction in outer hoop stress (thick green arrows) compared with the static hoop stress but not always a corresponding increase in outer airway wall radius. In contrast, the *protocol 2* mean dynamic outer radii (magenta loops) increase significantly from the static case (grey circle) and in proportion to ΔP_{TM} (magenta arrows), but the change in mean stress is relatively small. At the lumen (Fig. 4*B*), however, the modification to the pressure isoline for *protocol 1* (open black circles) does not follow the downward shift seen at the outer radius. Application of P_{TM} oscillations at low agonist causes an increase in hoop stress (right-most green arrow) in contrast with the higher agonist loops (left-most green arrows).

The stiffness of the airway wall varies from lumen to outer wall and depends on agonist level. The contrasting behavior between the lumen and outer wall can be explained by comparing the static stiffness of the airway wall for low and high agonist levels (Fig. 5) and between lumen and outer wall (yellow vs. green curves in Fig. 5, *A* and *B*). We observe that the stiffness curves are shifted dramatically at high agonist levels (Fig. 5*B* compared with Fig. 5*A*) and that the stiffnesses at the selected P_{TM} points vary significantly between low and high agonist levels and between lumen and airway wall (com-

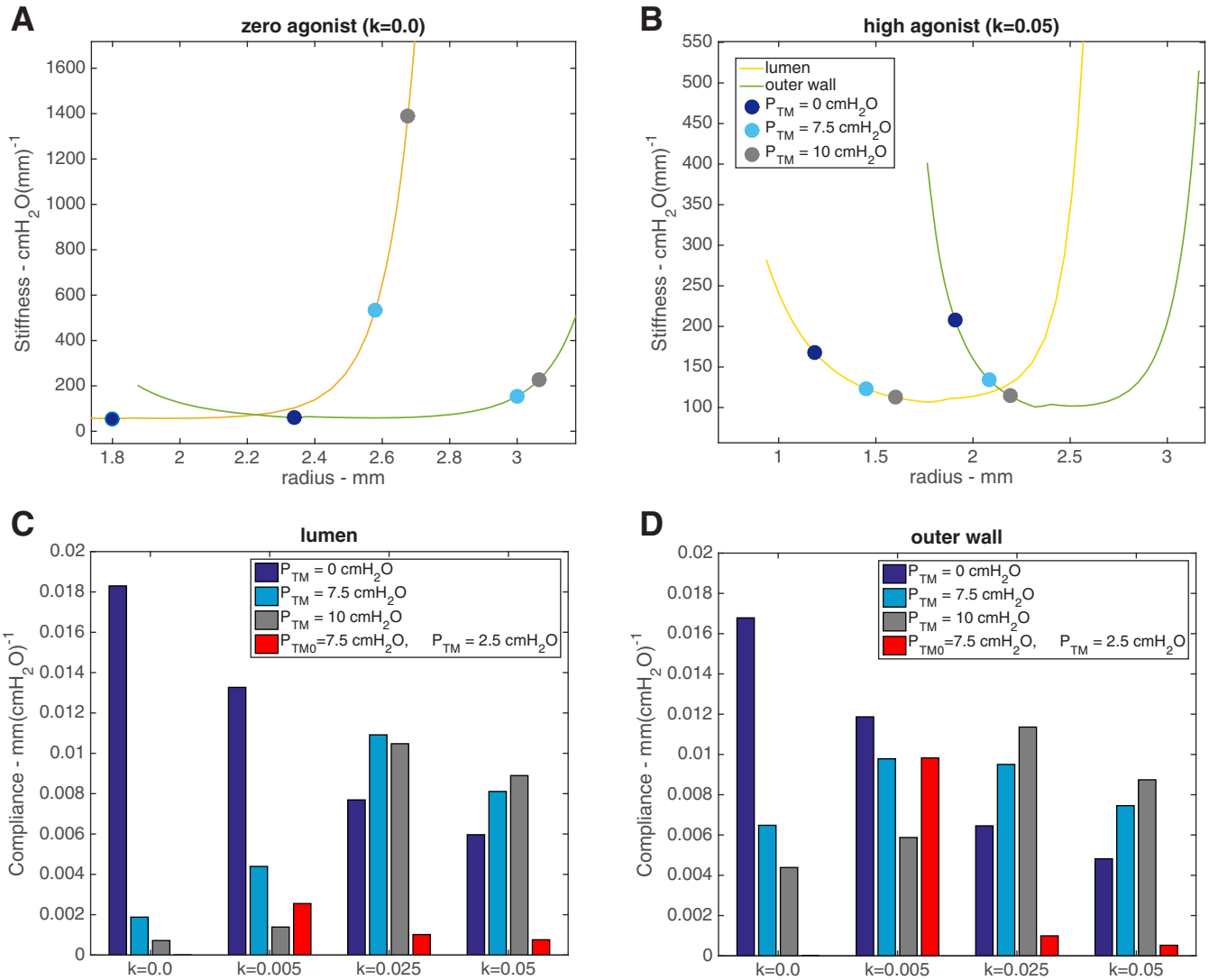

Fig. 5. *A* and *B*: static stiffness at the lumen plotted as a function of the lumen radius (yellow curves) and the static stiffness at the outer wall plotted as a function of the outer wall radius (green curves) for zero agonist (*A*) and application of the highest agonist level (*B*) ($k = 0.05$). The stiffness is determined by calculating the slope of the stress-radius curves in Fig. 4. Solid blue, cyan, and grey circles indicate the static stiffness at static $P_{TM} = 0$, 7.5, and 10 cmH_2O, respectively. Lumen (*C*) and outer wall (*D*) compliances (the reciprocal of the slope of the stress-radius curves) for each agonist level used in *protocol 1* simulations, for $P_{TM} = 0$, 7.5, and 10 cmH_2O (blue, cyan and grey bars, respectively) and dynamic compliances (red bars) for each agonist level resulting from application of P_{TM} fluctuations about $P_{TM0} = 7.5$ cmH_2O. The dynamic compliances shown here are calculated by determining the reciprocal of the mean slope of the green loops (*protocol 1* simulations) in Fig. 4.

pare cyan circles between Fig. 5, *A* and *B*). The effect of P_{TM} oscillations on the compliance of the airway wall is evident in Fig. 5, *C* and *D*. At higher agonist levels, at both the lumen and outer wall, there is a marked decrease in mean dynamic compliance relative to the static compliance (red bars compared with cyan bars in Fig. 5, *C* and *D*). Therefore, in particular, although there is a small increase in outer wall radius (left-most green loops in Fig. 4*A*), the airway wall in this region has become very stiff and therefore cannot admit large changes in radius in the final oscillatory solution. The magnitude change in mean hoop stress appears not to depend strongly on the degree of activation, which may be explained by it being offset by the significant decrease in compliance (Fig. 5*D*). The only case where oscillatory dynamic loading leads to a compliance that is similar to that of the static case is at the outer wall for the lowest agonist level. The contrasting behavior between the airway wall at the lumen and at the outer wall is thus a result of the complex interaction between the contractile force and effective nonlinear behavior of the different regions of the activated airways (Fig. 5, *A* and *B*). This is a consequence of the circular geometry and finite thickness of the airway wall.

Structural heterogeneity in ASM density exaggerates stress heterogeneity across the airway wall. So far we have assumed a uniform density of ASM fibers across the airway wall. However, histological lung sections and precision-cut lung slices show localization of ASM muscle bundles closer to the lumen than the outer wall. We therefore modify the parameter β, which accounts for the density of ASM fibers per unit volume in the airway model (see *Eq. S33* in the Supplemental Material of Ref. 10), to a function of the undeformed radius so that $\beta(R)$ now describes a nonuniform distribution of ASM across the airway wall (orange curve in Fig. 6*A*). To maintain consistency with previous results, we have chosen the parameters in describing $\beta(R)$ to ensure that the area under the curve (total amount of ASM) matches that of the uniform case (blue

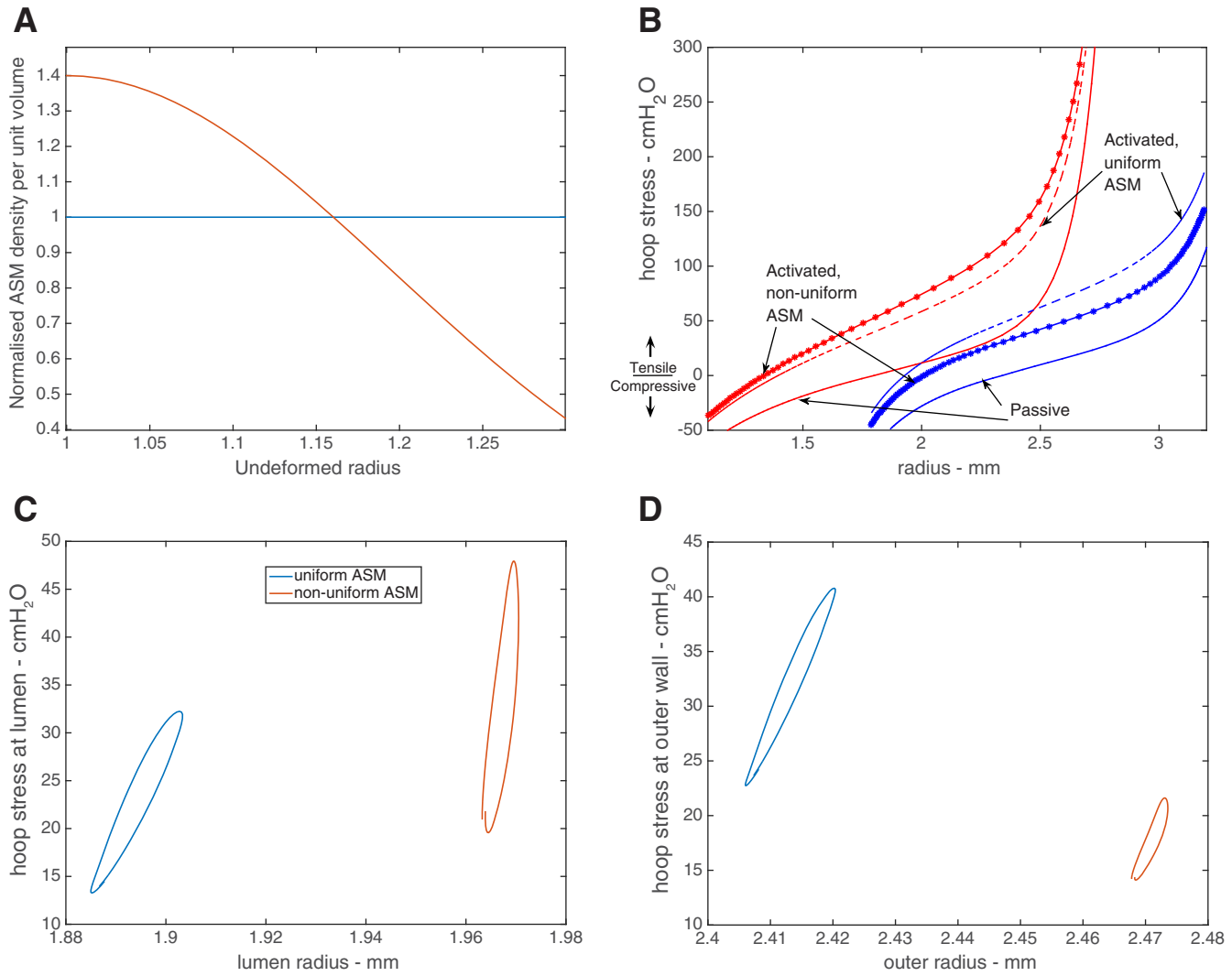

Fig. 6. *A*: normalized ASM density per unit volume within the airway wall plotted as a function of normalized airway wall radius representing a uniform distribution of ASM across the whole layer (blue curve) and localization of ASM closer to the lumen in which the distribution $\beta(R) \propto \exp[-13.1(R - R_a)^2]$ (orange curve). *B*: static internal (red curves) and external (blue curves) stress plotted as a function of lumen and outer radius respectively, for passive airways (solid), activated uniformly distributed ASM (dashed) and activated nonuniformly distributed ASM (dot dashed). *C*: *protocol 1* dynamic lumen hoop stress-radius loops for uniform ASM (blue) and nonuniform ASM (orange). *D*: *protocol 1* dynamic outer hoop stress-radius loops for uniform ASM (blue) and nonuniform ASM (orange). All activation is with $k_1 = 0.025\ s^{-1}$.

curve in Fig. 6*A*). Quasistatic lumen and outer wall stress-radius curves for increasing transmural pressure (Fig. 6*B*) show that hoop stress heterogeneity in the activated airway (k_1 = 0.025 s^{-1}) is further exaggerated for the nonunifom case compared with the uniform case. The exaggeration in stress heterogeneity persists on application of P_{TM} oscillations (*protocol 1*, k_1 = 0.025 s^{-1}) as shown in Fig. 6, *C* and *D*. At the lumen, the pressure fluctuations drive greater bronchodilation (Fig. 6*C*), presumably because the oscillatory strain is imposed on a greater proportion of the ASM near the lumen compared with the uniform case. However, at the lumen, the mean hoop stress and regional stiffness (mean slope of the stress-radius loop) are greater in the nonuniform (orange loop in Fig. 6*C*) than in the uniform case (blue loop). In contrast, at the outer radius, the mean hoop stress is less in the nonuniform case (Fig. 6*D*) but appears to exhibit similar regional stiffness to the uniform case. These findings suggest that the tissue strip should be taken much closer to the lumen where the muscle is located.

Comparisons of Intact Airway Model Predictions with Tissue Strip Model Simulations

Our model provides us with a tool to investigate, in silico, the effect of different loading conditions and the in vivo environment on the intact airway and the tissue strip. The simulations outlined below use parameter values given in Table 1. The strain amplitudes from the airway simulations are applied as static or oscillatory stretches to the tissue strip. The stretch of fibers located at different radii across the airway wall is not uniform. We therefore determine the stretch experienced by fibers in the middle of the airway wall, apply this stretch to the strip (effectively taking the strip to the same in situ length as in the airway at the start of the simulation), and then compare stresses (Fig. 2). It is likely that the process of isolating the airway strip requires removal of some ECM associated with the basement membrane. Comparisons are therefore also made to a modified strip for which the density of the ECM and ASM fibers is decreased and increased, respectively, by 50%.

Although identical stretches are applied to both strip and airway, the longitudinal stress in the strip resembles the hoop stress only at the outer wall of the airway. The hoop stresses at the inner and outer boundaries of the airway wall are compared with the longitudinal stress along the tissue strip in Fig. 7. The curved geometry of the intact airway generates stress heterogeneity across the airway wall [Fig. 3; Brook et al. (4)]. Therefore, in the initial stressed state the hoop stress is greater at the inner boundary (red curves in Fig. 7, *A–C*), while with a sufficiently large concentration of agonist the hoop stress is greater at the outer boundary (green curve). Although the stretch applied to the tissue strip is equal to the stretch at the mid point of the airway wall, the stress within the strip (blue curves) resembles the hoop stress at the outer boundary of the airway wall and falls within the range of stresses experienced by the intact wall (Fig. 7, *G* and *J*). For *protocol 2*, the hoop stress at the inner boundary of the wall is sometimes compressive for part of the steady oscillatory loops, indicating stress heterogeneities within the wall, with the inner part experiencing compressive stresses while the outer part experiences tensile stresses. It is also possible for the stress within the strip to be compressive, as seen in Fig. 7*K*, but not heterogeneous. Larger amplitude stretches result in greater hysteresis (Fig. 7, *D*, *K*, and *L*).

At high agonist levels, longitudinal stresses in the modified tissue strip are greater than hoop stresses in the airway wall. Also plotted in Fig. 7 is the longitudinal stress in a modified tissue strip (black curves), for which the collagen and ASM volume fractions are, respectively, decreased and increased by 50%. For both protocols when the strips are agonist-free, the reduced collagen fraction in the modified strip leads to a smaller stress (Fig. 7, *A–C*). This behavior is modified in the presence of agonist. For *protocol 1*, as the strip is activated and contracts, the contribution of the collagen to the stress reduces exponentially, with smaller reduction in the modified strip, except when the smooth muscle is contracted and the collagen does not contribute to the stress. However, there are greater increases in the stress due to contributions from the ASM in the modified strip as k_1 increases. In contrast, as k_1 increases in the original strip, the stress due to ASM forcing is never dominant so there is a reduction in the stress (blue curves in Fig. 7, *A*, *D*, *G*, and *J*). At the highest agonist level both strips are sufficiently contracted for the collagen to have no effect and the increased ASM content of the modified strip results in a greater stress.

For *protocol 2* (g_1 = 0.1), in the contracted state the fibers are compressed, and small amplitude oscillations (1.25, 2.5 cmH_2O; Fig. 7, *E–H*) result in insufficient collagen recruitment and so contribute little to the resultant stress. Further increase in oscillation amplitude increases the range of stretch giving rise to increased disruption of cross-bridge cycling so there is more hysteresis. At the same time, however, increased stretch causes collagen recruitment, leading to an increase in the peak stress (Fig. 7*K*). When g_1 = 0.01 the smooth muscle remains contracted (e.g., compare range of resultant stretch between Fig. 7, *K* and *L*) for all the amplitudes of pressure oscillations, with an increase in hysteresis as the oscillation amplitude increases (Fig. 7, *F*, *I*, and *L*).

For identical oscillatory stretches, mechanical loads experienced by ASM within the airway wall are not identical to those experienced by ASM in the tissue strip. We now compare the predicted static radii and hoop-stresses of the airway (red circles in Fig. 8*A*) with equivalent tissue-strip length and static longitudinal stresses (green diamonds in Fig. 8*A*) under increasing agonist. If strips are subjected to fixed-amplitude length oscillations (green arrows in Fig. 8*A*) under increasing agonist, the operating points (green diamonds) are at very different parts of the stress-strain curve to those in the intact airway (red circles) and therefore have different baseline stiffness or compliance. Applying fixed-amplitude force oscillations (blue arrows in Fig. 8*A*), for increasing agonist, gives operating points indicated by the blue squares in Fig. 8*A*, which are closer to the intact airway (red circles). However, both force- and length-oscillations in the strip (green and blue arrows) will not necessarily follow the initial path followed by applying pressure oscillations as indicated by the red arrows in Fig. 8*A*. These differences are further magnified when compared with the stress-radius curves at the lumen. Experimental measurements, however, focus on lumen radius, where the hoop stresses are significantly different to those in the tissue strip and for which the behavior departs from that of the outer wall (Fig. 4*A*). In an attempt to more accurately mimic appli-

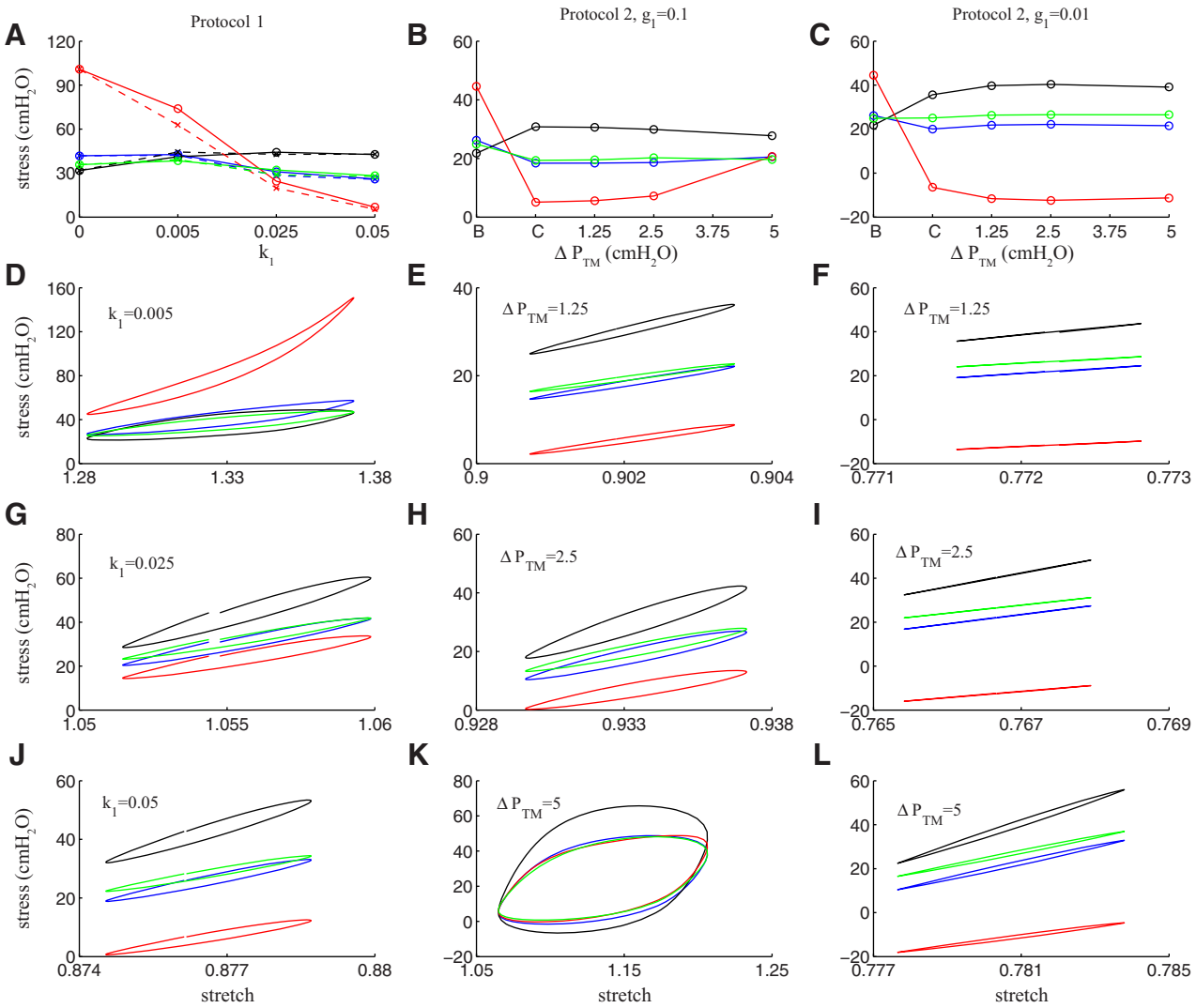

Fig. 7. Plots of the dynamic hoop stress as a function of dynamic stretch (resulting from application of P_{TM} fluctuations) at the inner (red) and outer (green) boundaries of the airway wall and longitudinal stress in a tissue strip (blue) plotted as a function of k_1 (*A*) and ΔP_{TM} (*B* and *C*). In *B* and *C*, B on the *x*-axis refers to the baseline (initially prestressed) state (cyan circle in Fig. 4) and C refers to the contracted state i.e., after application of agonist (grey circle in Fig. 4). Also plotted is the resultant stress in a modified strip (black) i.e., when the influence of the ASM and collagen are respectively increased and decreased by 50%. All the resultant stresses (at the lumen, outer radius and in the strip) are reported as functions of the stretch applied at the mid-line of the airway thus allowing the loops to have the same *x*-axis range and enabling effective comparison of the corresponding magnitude of stress. The *A*, *D*, *G*, and *J*: results for *protocol 1*, with the dashed and solid lines indicating the static and tidal transmural pressures (respectively). Dynamic force-length loops for a single pressure oscillation are shown for $k_1 = 0.005$ (*D*), $k_1 = 0.025$ (*G*), and $k_1 = 0.05$ (*J*). Results for *protocol 2* are shown for either $g_1 = 0.1$ (*B*, *E*, *H*, and *L)* or $g_1 = 0.01$ (*C*, *F*, *I*, and *L*): a parameter that governs the strain-dependent detachment of so-called latch bridges (in the HHM model). Dynamic force-length loops for a single pressure oscillation are shown for $\Delta P_{TM} = 1.25$ cmH_2O (*E* and *F*), $\Delta P_{TM} = 2.5$ cmH_2O (*H* and *I*), and $\Delta P_{TM} = 5$ cmH_2O (*K* and *L*). Note that for dynamic cases the stress is plotted at the end of a complete oscillation.

cation of transmural pressure oscillations, which were neither length nor force driven (auxotonic load driven), to tissue strips, Latourelle et al. (22) predicted theoretical force-length characteristics to drive a servo-controller in tissue-strip experiments (Fig. 8*B*). Their loading condition, however, was based on the semi-empirical pressure-radius relationship of Lambert et al. (18) and the Laplace approximation for thin walls. We can make a direct comparison between the load characteristics of Latourelle et al. (22) by extracting the equivalent forces and lengths from our model predictions (red and blue curves in Fig. 4), which are shown in Fig. 8, *C* and *D*. The Latourelle et al. (22) results show a universal decrease in force with increase in length characterized by the sigmoidal curves in Fig. 8*B*. In contrast, load characteristics at the lumen (Fig. 8*C*), predicted by our model, show a universal increase in hoop stress with increase in length. The load characteristics at the outer wall in Fig. 8*D* from our model are qualitatively similar to the curves in Fig. 8*B* for $P_{TM} = 0$ and 2.5 cmH_2O but more generally reveal the complex behavior discussed above, resulting from interactions between internally generated forces by the ASM and strain-stiffening of collagen.

In summary, for identical oscillatory stretches, the tissue strip fails to replicate the mechanical behavior of the inner wall. The similarity in outer-wall hoop stress of the airway and that of the unmodified strip suggests that the effect of increasing agonist for auxotonic loading conditions (where neither

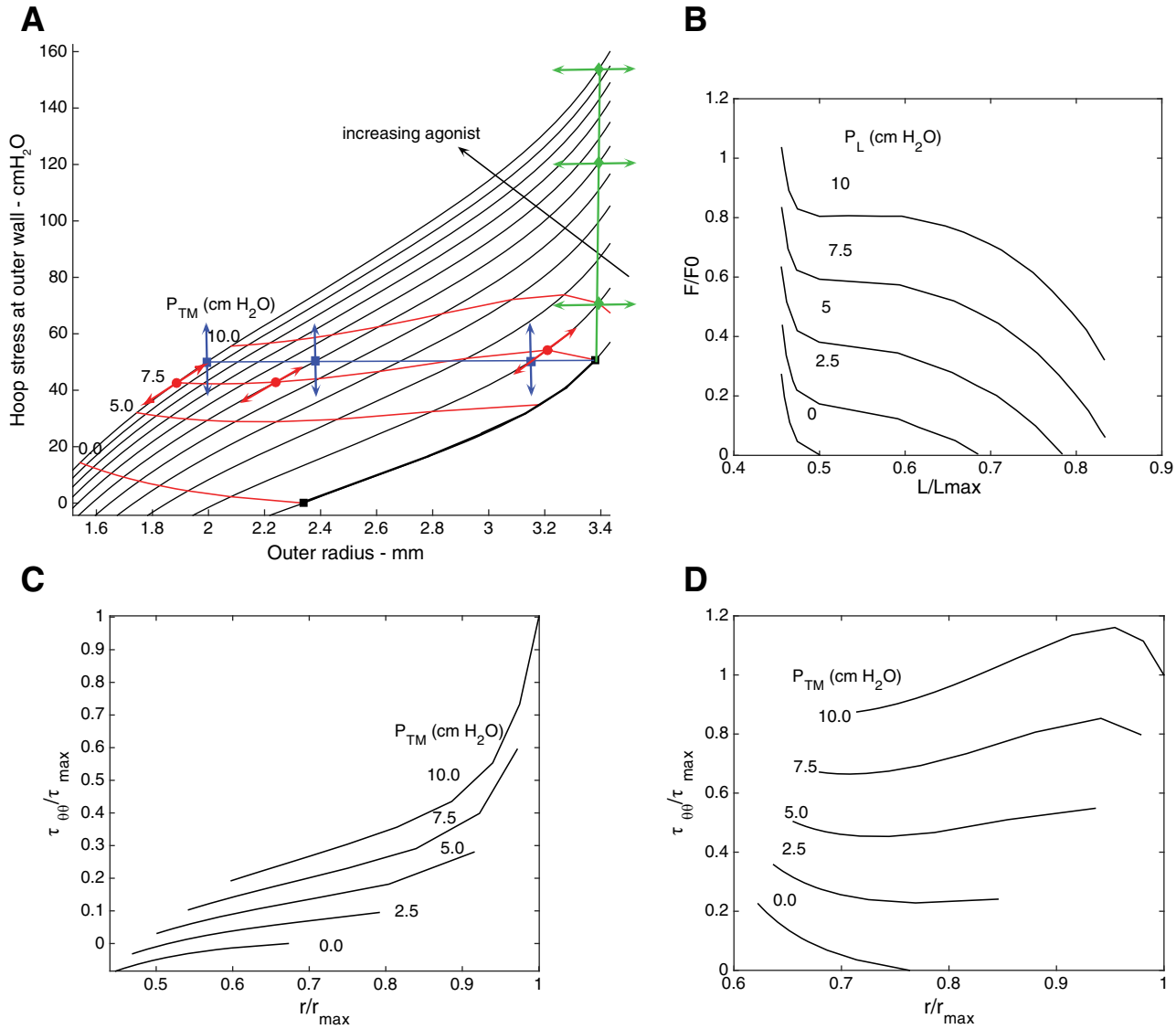

Fig. 8. *A*: hoop stress at outer wall plotted as a function of outer radius for increasing agonist (black curves) as in Fig. 4*A*, with transmural pressure isolines (red curves). Lowest black square is hoop stress and outer radius in the undeformed, unactivated state. Heavy black curve on the zero agonist curve indicates change in hoop stress and outer radius as a result of increasing transmural pressure from 0 to 7.5 cmH_2O in the unactivated airway. Green diamonds indicate longitudinal stress that would be applied to a tissue strip held at fixed length in the presence of increasing agonist (isometric experiments); green arrows indicate initial paths that may be taken to apply length oscillations. Blue squares indicate operating points of longitudinal stress and tissue-strip length, for a strip under a fixed load (isotonic experiments) in the presence of increasing agonist; blue arrows indicate initial paths that may be taken to apply force oscillations. Solid red circles indicate operating points of hoop stress and outer wall radius in the presence of increasing agonist for fixed static transmural pressure for which both force and radius vary (auxotonic loading) along the initial paths indicated by the red arrows. *B*: force-length load characteristics predicted by Latourelle et al. (22) for an airway by assuming the pressure-radius relationship of Lambert et al. (18) and the Laplace approximation for thin walls (reproduced with permission from the American Physiological Society). F/F_o is the muscle force relative to optimal force; L/L_{max} is the muscle length relative to L_{max} (the length of relaxed muscle at a transpulmonary pressure of 30 cmH_2O). Equivalent stress-radius load characteristics for our model at the lumen (*C*) and the outer wall (*D*) (extracted from blue and red curves in Fig. 4) for P_{TM} ranging from 0 to 10 cmH_2O. τ_{max} And r_{max} are the hoop stress and radius, respectively, at either the lumen or at the outer wall at $P_{TM} = 10$ cmH_2O.

load nor length are held fixed) is more likely to be depicted by the pressure isoline curves shown in Fig. 4*A*. Identical stretches applied to the modified tissue strip further exaggerate differences between the mechanical behavior of the airway and the strip, with measurements of contractile force in the tissue strip potentially overestimating those that may occur in the airway. These results strongly suggest that the nonlinear strain-stiffening effect of the extracellular matrix in the in vivo environment contributes to the integrated dynamic response of the airway to pressure oscillations, which the modified tissue strip fails to replicate.

DISCUSSION

To understand mechanisms underlying AHR in asthma, we have previously developed and validated a multiscale model of an intact airway embedded in parenchyma accounting for helical ASM and collagen fibers within the nonlinear elastic

matrix of the tissue in the airway wall (10). Contractile force generated by ASM cells is determined via the HHM model for subcellular cross-bridge dynamics and is dynamically coupled to the tissue mechanics through the embedded ASM fibers, significantly extending previous airway models (17, 19, 22, 26, 33, 30). In our previous study (10) we showed that the application of transmural pressure to the activated airway dictated the effective static stiffness of the airway wall. In turn, higher effective airway stiffness was shown to limit the amount of strain that could be transmitted to the contractile machinery in the ASM cell, limiting the degree of bronchodilation that could be achieved. In the present study we have additionally developed a model for a tissue strip, which is assumed to have identical material properties to that of the intact airway, with longitudinally embedded ASM and collagen fibers. This work allows us to understand the effect of quasistatic and dynamic pressure changes, the combined role of actin-myosin dynamics and nonlinear tissue-level mechanics in generating internal stresses in the intact airway (currently inaccessible via experiment), and how these compare with the stress in a tissue strip. It also allows us to fully explore the effect of geometry on the micromechanical environment that may exist in the intact airway.

ASM Force Generation and Collagen Recruitment Contribute to Stress Heterogeneity in the Airway Wall

We find the resultant hoop stresses in the airway wall are heterogenous across the airway wall [in agreement with the linear-elastic model predictions of Brook et al. (4) and illustrated above; Figs. 3 and 4]. Furthermore, the nature of the heterogeneity varies significantly with agonist concentration (with the lumen hoop stress greater than at the outer boundary at low agonist concentrations but lower at high agonist concentrations; Figs. 3 and 7*A*) and hardly varies for increasing amplitude of pressure fluctuations for small g_1, i.e., for low detachment rate of latch bridges (Fig. 7*C*). The decrease in stress with increase in agonist concentration (Fig. 4*C*) is counterintuitive at first glance. To explain this, we note that as P_{TM} is increased for the unactivated airway (moving up the zero-agonist curve in Fig. 4*B*), the lumen hoop stress increases significantly; for the same strain and applied P_{TM}, the lumen hoop stress is greater than the hoop stress at the outer wall (Fig. 4*B*, *inset*) and places the lumen radius on a much stiffer part of the stress-strain curve (Fig. 5). Consequently, although agonist increases contractile force, it causes only a small reduction in lumen radius.

This behavior is a direct consequence of the fact that airway radius cannot be held at some fixed value (as tends to be done in isometric tissue-strip experiments), so that as the airway contracts (from an initially stretched state), the stretch experienced by the airway moves from where collagen stiffness dominates (Fig. 7*D*), to a point where collagen is derecruited (Fig. 7*J*), so that the mid-point of the stretch oscillation moves down the stress-strain curve (Fig. 4). Given that the stress-strain curve combines the effect of stiffening due to collagen recruitment at large transmural pressures and stiffening due to contraction at lower transmural pressure, this change in "operating" radius is more likely to occur in vivo and is not accounted for in tissue strip experiments. Indeed, at a fixed operating length, increasing agonist concentration would result in increased hoop stresses. Furthermore, the same mechanism causes the mid-point of the stretch oscillation in the airway wall to increase with increasing amplitude of oscillation for larger latch-bridge detachment rate, g_1 (Fig. 7, *E–K*), thus moving up the stress-strain curve, and therefore to an effectively stiffer airway. This explains the increase in stress for increasing amplitude pressure fluctuations (Figs. 4*B* and 7*B*); the balance between contributions due to ECM stiffness and contracted ASM stiffness shifts from the latter to the former. The almost flat stress curves for smaller latch-bridge detachment rate g_1 (Fig. 7*B*) are a result of the stretches remaining well below the collagen recruitment threshold (Fig. 7, *F–L*).

Furthermore, our model predicts that structural heterogeneities, such as those that arise from localization of ASM bundles closer to the lumen, exaggerate quasistatic and dynamic stress heterogeneities across the airway (Fig. 6). This appears to be a consequence of transmission of strain to a greater proportion of the activated muscle (as this is located closer to the lumen) in the isolated airway, under the protocol simulated here whereby P_{TM} fluctuations are imposed by applying internal pressure oscillations. Whether or not this would be the case if P_{TM} fluctuations are imposed through application of external pressure oscillations (which may be closer to what occurs during tidal breathing in vivo) requires further theoretical and experimental investigation.

Taken together these results strongly suggest that the nonlinear strain-stiffening effects of the extracellular matrix in the in vivo environment play a hitherto underappreciated role in the integrated response of the airway to pressure oscillations, which the tissue strip fails to replicate.

ASM Force Generation and Collagen Recruitment Contribute to Compliance Heterogeneity in the Airway Wall

The counterintuitive observations above are a result of intricate relationships between strain stiffening at high transmural pressure and the effect of airway narrowing at high agonist levels. We can effectively capture the interrelationships by considering regional compliance, which is a measure of the amount of stretch required to generate a hoop stress at a particular location (Fig. 5). The heterogeneity in stiffness (resulting from different hoop stresses at the lumen compared with those at the outer wall) is readily observed in Fig. 5, *A*, *C*, and *D* where the given increases in transmural pressure result in different static stiffnesses at the lumen compared with the outer wall. In contrast, application of agonist causes a shift of the static stiffness-radius curves to the right, which, in combination with the nonlinearity of the static stiffness-radius curves, causes a decrease in stiffness at both the lumen and outer wall for the given increases in transmural pressure (Fig. 5, *B–D*). Furthermore, there is evidence of heterogeneity in the dynamic compliances; pressure fluctuations cause a significant reduction in compliance at the lumen for all agonist levels (Fig. 5*C*) but only at higher agonist levels at the outer wall (Fig. 5*D*). A growing body of research (16, 25, 32) has shown that vascular smooth muscle cells and fibroblasts migrate up stiffness gradients and therefore the heterogeneities we have highlighted here may be implicated in structural remodeling of the airway.

Matching Pressure Fluctuations Experienced by the Airway Wall to Length Fluctuations in the Tissue Strip

To investigate the role of tidal breathing and deep inspirations (DIs) in modulating AHR, numerous experimental studies have involved application of length and force oscillations to ASM strips (6, 22, 29, 34) and volume and pressure oscillations to isolated, intact airways (21, 28). Length oscillations applied to strips were shown to significantly decrease contractile force, a response which has been attributed predominantly to disruption of cross-bridge cycling (7, 27). In contrast, transmural pressure oscillations and DIs applied to intact airways appear to have only limited bronchodilatory effect (21, 28). However, DIs at the whole organ level in vivo have been shown to have a strong bronchodilatory effect (2, 24). To identify which components of the mechanical environment present in the airway (but absent in the tissue strip) may contribute to these discrepancies, in this work we have applied identical stretches to both and compared the resulting stresses. Due to the assumed circular geometry of the airway wall, as the airway deforms, the fibers at different positions within the airway wall experience different amounts of stretch. In contrast, a uniaxial stretch applied to a tissue strip, for which all of the fibers are parallel, results in a uniform stretch in all of the fibers. To make comparisons between the two geometries we used the fiber at the mid-point of the airway wall as a reference. The stretches, in the middle of the airway wall, that result from applying either static transmural pressure or dynamic transmural pressure fluctuations to the airway wall are thus applied to the tissue strip model and the resulting longitudinal stresses in the strip are determined and compared with hoop stresses in the airway wall. In this way we have translated the pressure fluctuations experienced by an airway wall to application of identical length fluctuations to a tissue strip, thus eliminating one of the implicated confounding factors. We therefore suggest that to mimic the pressure fluctuations better, the tissue strip experiments should be guided by the auxotonic curves at the outer wall (Fig. 8*D*) since the stresses in the tissue strip are similar only to the outer wall stresses when the same stretches are applied (blue and green curves/loops in Fig. 7). That is, the length oscillations need to be applied to increasing lengths for increasing agonist to mimic zero transmural pressure but applied to decreasing lengths for increasing agonist to mimic transmural pressure of 10 cmH_2O (Fig. 8*D*).

Stress Heterogeneity in the Airway Wall Significantly Affects Predictions of Auxotonic Loading Conditions

The variation of stress heterogeneity across the airway wall with increasing agonist concentration makes the difference in stress between the tissue strip and the airway even greater (Figs. 7, *D*, *G*, and *H*, and 8). If the tissue-strip stretch were fixed and length oscillations applied about this reference length, we would see a dramatic increase in stress and a shift to more compliant parts of the stress-strain curve, in contrast with the decrease in hoop stress predicted for the auxotonic loading conditions that may operate in vivo (Fig. 8). Latourelle et al. (22) attempted to mimic the auxotonic loading conditions that may exist in vivo by using a model-based loading condition to drive a servo-controller to apply oscillations to tissue strips that were neither length nor force driven. Their loading condition, however, was based on the semi-empirical pressure-radius relationship of Lambert et al. (18) and the Laplace approximation for thin walls, which fails to account for the stress heterogeneity across the finite-thickness wall, resulting in isopressure curves that do not reflect the interactions of active and passive forces seen here and so depart significantly from those predicted with the present model (Fig. 8). Our model simulations also suggest that stress heterogeneities are further exaggerated in thickened airway walls that may occur as a result of airway remodeling (results not shown). We suggest that future experimental studies on tissue strips should utilize loading characteristics for both the lumen and outer wall as predicted here to deliver oscillations that mimic more closely the in vivo situation and therefore to obtain more realistic tissue response.

Potential Effects of Stress Heterogeneity on Airway Remodeling

The large compressive stresses at the lumen (Fig. 7, *A* and *C*) predicted above are, in part, a consequence of the inherent assumption in the model that ASM and collagen fibers are uniformly distributed across the airway. If the distribution of these were heterogeneous, so that collagen fiber density is higher near the lumen than at the outer wall, then the stress and compliance heterogeneity may be reduced. Indeed it seems unlikely that cells can reside in such heterogenous micromechanical environments (11), raising important implications for tissue homeostasis and mechanotransduction, suggesting that airway remodeling [e.g., via ASM proliferation and collagen deposition (14) or recruitment of myofibroblasts up stiffness gradients (32)] may be driven by the necessity to reduce stress heterogeneity, potentially resulting in heterogenous fiber density distributions (13, 31, 35). Imaging studies such as those of Clifford et al. (5), which utilize three-dimensional confocal microscopy to visualize ECM within the walls of pressurized blood vessels, could be a powerful tool for determining spatial distributions of ECM and ASM fiber density in the airway.

Model Limitations

We have assumed an axisymmetric geometry for the airway, which is unrealistic especially in strongly contracted airways where large compressive forces are likely to cause buckling and mucosal folding and thus modify the micromechanical stress environment. Additionally, the basement membrane, with its high collagen content, has not been explicitly modelled here. Instead we have opted to focus on the stress distributions within the stiffer smooth muscle layer (with its active components). An inner (passive) mucosal layer could be added in future studies, within which stress distributions would be modified to some extent. However, the mucosal layer is relatively soft compared with ASM and other wall components, so while the deformations might be quite dramatic, they may not have a major role on the overall airway stiffness. As it stands the stress predictions from the current model predict onset of buckling (as regions of compressive stress), which also depends on the relative stiffness of the muscle and mucosal layer (36). Buckling at the inner wall can be anticipated for $P_{TM} = 0$ near the inner wall (Fig. 4), where the stress becomes strongly compressive; the effect of buckling near the inner wall would likely be to reduce the magnitude of the compressive

stress locally, without significantly altering tensile stress predictions elsewhere.

We have shown that structural heterogeneity in the ASM fiber density (with greater ASM nearer the lumen than the outer wall) appears to further exaggerate stress heterogeneities predicted under the assumption of uniform fiber densities. We have, however, had to limit the heterogeneity in fiber density to having a small gradient. We believe that steeper gradients in smooth muscle distribution may violate technical criteria that the underlying solid mechanics have to satisfy (such as convexity of the strain energy), demanding more profound adjustment to the model; this refinement will be considered in future studies.

Although we have modelled a generic airway (potentially from any part of the tracheo-bronchial tree), we have previously validated the model behavior specifically against experiments from LaPrad et al. (21) [details are given in Hiorns et al. (10)]. The pressure-radius curves of the airways from their study indicate the presence of a passive strain-stiffening effect that is likely to come from collagen as the main constituent of connective tissue in airways. By fitting the nonlinear elasticity parameter values C_1 and C_2 to their passive pressure-radius curves, we are able to identify behavior specific to the airways they used in their study. In any case, ECM is present in essentially all tissues so there will always be some effect of the strain-stiffening behavior of collagen, the extent of which will almost certainly be generation dependent. Passive pressure-radius curves for airways from different generations could be used (e.g., Refs. 9, 18) to apply our model more generally and to integrate models of many airways in into a branching network, which will potentially have different effective pressure-area and stiffness-area curves when activated.

There is considerable evidence that cells sense and respond to their mechanical environment (11) (and references therein); the internal stresses that are generated through cell-tissue interactions as demonstrated in this study are therefore likely to feed back to the contractile machinery, cytoskeleton, cell-cell, and cell-ECM interactions. This mechanical feedback from macro- to microscale, which plays an important role in mechanotransduction, has not been accounted for here but will be considered in future studies. An important limitation is that internal stresses in the airway wall are currently difficult to access experimentally, and so this work has not been validated by direct comparison with measured data. However, we have carefully validated the airway model (10) against isolated intact airway experiments (21) and shown good agreement between simulation and experimental data for both static and dynamic airway airway caliber and thickness; the simulated stresses are thus predictions that we believe to be reasonably realistic subject to the limitations already mentioned.

Given that the debate on the role of deep inspiration on modulating hyperresponsiveness has revolved around extrapolations of cell-level and tissue-strip behavior, we believe that our tissue-level airway model that incorporates more of the in situ factors as well as accounting for dynamic cell-level effects suggests some useful new hypotheses. Whether or not these hypotheses are confirmed requires further experiments and more detailed modeling studies.

Summary

In this work we have shown that the competition between passive properties of the ECM and the dynamically varying forces generated by the ASM, together with the circular geometry of the intact airway, plays an appreciable role in generating P_{TM}-dependent hoop-stress heterogeneities across the airway wall. These yield counterintuitive auxotonic stress-radius load characteristics that differ significantly both qualitatively and quantitatively between the lumen and the outer wall of the airway. Stress heterogeneities also result in compliance heterogeneity, capturing the contrasting stress-strain behavior between the lumen and outer wall and providing a mechanistic explanation for our counter-intuitive predictions. In particular, by accounting for both ECM and dynamic ASM behavior we are able to compare dynamic hoop stresses generated in the airway wall (not currently amenable to experimental observation) with corresponding stresses in the tissue strip more accurately than previously possible. In doing so we conclude that, in tissue-strip experiments (even under auxotonic loading conditions), airway smooth muscle within the strip is subject to stresses that resemble the stress only at the outer boundary of the airway wall (not an average value as estimated by Laplace laws) and completely fail to replicate the stress environment near the lumen. We therefore suggest that if the tissue strip experiments are to represent the airway wall, then loading to the strip should utilize auxotonic loading characteristics at the outer wall. Corresponding lumen behavior can then be predicted by appropriate use of the present model of a finite thickness airway. We have also shown that any modifications to the ECM content of a tissue-strip could further exaggerate the difference between stresses experienced by ASM cells in the tissue strip compared with those in the intact airway. We currently have little knowledge of how ASM cells respond to these stresses, but these should be investigated if we are to extrapolate observations from isolated tissue experiments to behavior in vivo. We thus suggest that the role of these stress heterogeneities in the development of AHR should be explored further both theoretically and experimentally.

APPENDIX: MODEL OF TISSUE STRIP

We assume that the tissue strip is long and thin, since the strips used by Fredberg et al. (6) measured $2 \times 3 \times 20$ mm. Any boundary layers due to clamping are ignored, since the length is much greater than the height and width, which are roughly equal.

A strip of unstressed equilibrium length L_u, subject to uniaxial strain, is considered, so that

$$x = \lambda_1 X, y = \lambda_1 Y, s = \lambda S, \quad (A1)$$

Here X, Y, S are Lagrangian Cartesian coordinates and x, y, s are coordinates in the deformed configuration. (S is used so as not to be confused with Z in the airway.) The deformation gradient tensor, $\mathbf{F} \equiv$ Grad x is given by

$$[\mathbf{F}] = \begin{pmatrix} \lambda_1 & 0 & 0 \\ 0 & \lambda_1 & 0 \\ 0 & 0 & \lambda \end{pmatrix}. \quad (A2)$$

Assuming incompressibility, $\lambda\lambda_1^2 = 1$, implying that $\lambda_1 = 1/$Therefore, the left and right Cauchy Green stress tensors, $\mathbf{B} \equiv \mathbf{F}\mathbf{F}^T$ and $\mathbf{C} \equiv \mathbf{F}^T\mathbf{F}$, are given by

$$[\mathbf{B}] = [\mathbf{C}] = \begin{pmatrix} 1/\lambda & 0 & 0 \\ 0 & 1/\lambda & 0 \\ 0 & 0 & \lambda^2 \end{pmatrix}. \quad (A3)$$

In our previous model of the airway wall (10), we assumed an incompressible Neo-Hookean material embedded with two sets of helical fibers symmetrically disposed about the circumferential direction. These fibers have two functions; they produce a contractile force from activated ASM and during inflation they stiffen the airway to mimic collagen. Here, both sets of fibers are assumed to be aligned to the *s*-axis of the strip to mimic "cutting" of the strip from the original airway, so that the undeformed directions of the two sets of fibers are given by $\mathbf{M}_1 = \mathbf{M}_2 = \mathbf{e}_s$. In the deformed configuration $\mathbf{m}_1 = \mathbf{m}_2 = \lambda \mathbf{e}_s$.

The strain-energy function of a Neo-Hookean material is

$$W = \frac{\mu^{(a)}}{2}(\mathrm{I}_1 - 3), \quad (A4)$$

where $\mu^{(a)}$ is the shear modulus and $I_1 \equiv \mathrm{tr}(\mathbf{C})$ is the first strain invariant of $\mathbf{C}$. Two other terms are included in the strain-energy function to take into account the strain-stiffening and active force generation. As with our airway model (10), we use the anisotropic model of Holzapfel et al. (12) to take into account the fiber-stiffening, so that

$$W_{\mathrm{ani}}(I_4, I_6) = \frac{C_1}{2C_2} \sum_{f=4,6} H(I_f - 1)\{\exp[C_2(I_f - 1)^2] - 1\}. \quad (A5)$$

$C_1 > 0$ is a stress-like parameter taking into account the density of the fibers in the matrix, while $C_2 > 0$ is a dimensionless parameter that controls the nonlinear increase in the stiffness of the fibers as they stretch. The Heaviside function $H(I_f - 1)$ is included so that the collagen fibers are recruited only when stretched. The additional strain invariants are defined as $I_4 \equiv \mathbf{M}_1 \cdot (\mathbf{C}\mathbf{M}_1)$ and $I_6 \equiv \mathbf{M}_2 \cdot (\mathbf{C}\mathbf{M}_2)$, so that $I_4\, I_6 = \lambda^2$ are the square of the stretches of the fibers, which due to the symmetry are stretched equally.

We assume that the active force, *A*, generated by ASM cells within the fibers is only implicitly dependent on fiber stretch (via the HHM model for acto-myosin dynamics) and therefore is independent of I_4 and I_6; i.e., the stretch affects the applied velocity [which feeds into the HHM model (10)], which in turn modifies the distributions of the cross-bridge species and therefore affects the value of *A*. To ensure that the active component of the Cauchy stress tensor matches the general form described by Ambrosi and Pezzuto (1), namely

$$\tau_{\mathrm{act}} = A(\mathbf{m}_1 \otimes \mathbf{m}_1 + \mathbf{m}_2 \otimes \mathbf{m}_2), \quad (A6)$$

we model the active component of the strain-energy function as:

$$W_{\mathrm{act}} = \frac{A}{2}(I_4 + I_6). \quad (A7)$$

Determination of *A* at each time step of a length oscillation is based on the solution of the partial differential equations (PDEs) governing the HHM model for acto-myosin dynamics. The coupled system of equations are solved numerically, the full details of which are given in the Supplemental Material of Ref. 10.

By summing the Neo-Hookean, anisotropic and active contributions, we arrive at the same strain-energy function as was used for the airway wall (10), so that

$$W = \frac{\mu^{(a)}}{2}(I_1 - 3) + H(\lambda - 1)\frac{C_1}{C_2}(\exp[C_2(\lambda^2 - 1)^2] - 1) + A\lambda^2, \quad (A8)$$

with the Heaviside function in the middle term allowing recruitment of collagen fibers only when the strip is stretched $\lambda > 1$. The nonzero components of the Cauchy stress tensor are

$$\tau_{xx} = \tau_{yy} = -p + \frac{\mu^{(a)}}{\lambda}, \quad (A9)$$

$$\tau_{ss} = -p + \lambda^2(\mu^{(a)} + 2A) + H(\lambda - 1)4C_1(\lambda^2 - 1)\lambda^2 \exp[C_2(\lambda^2 - 1)^2]. \quad (A10)$$

Assuming that the sides of the strip are stress-free, $p = 1/\lambda$ and

$$\tau_{xx} = \tau_{yy} = 0, \quad (A11)$$

$$\tau_{ss} = \lambda^2(\mu^{(a)} + 2A) - \frac{\mu^{(a)}}{\lambda} + H(\lambda - 1)4C_1(\lambda^2 - 1)\lambda^2 \exp[C_2(\lambda^2 - 1)^2]. \quad (A12)$$

Conservation of momentum is satisfied and

$$x = \frac{X}{\sqrt{\lambda}}, y = \frac{Y}{\sqrt{\lambda}}, s = \lambda S. \quad (A13)$$

We assume that λ is prescribed as we apply length oscillations to match the strains applied to the airway via P_{TM} oscillations. To model application of force oscillations, τ_{ss} would be prescribed.

ACKNOWLEDGMENTS

We are grateful to Jeffrey J. Fredberg (Harvard School of Public Health) for helpful discussions.

GRANTS

J. E. Hiorns was supported by the Medical Research Council (MRC) Capacity Building Studentship Scheme (G0900197). B. S. Brook was supported by a New Investigator Research Grant funded by the MRC (G0901174) and partially supported by EU Seventh Framework Programme FP7/2007–2013 under grant agreement no. 270194 and is presented on behalf of the whole AirPROM consortium (www.airprom.eu).

DISCLOSURES

No conflicts of interest, financial or otherwise, are declared by the author(s).

AUTHOR CONTRIBUTIONS

J.E.H., O.E.J., and B.S.B. conception and design of research; J.E.H. and B.S.B. performed experiments; J.E.H. and B.S.B. analyzed data; J.E.H., O.E.J., and B.S.B. interpreted results of experiments; J.E.H. and B.S.B. prepared figures; J.E.H. drafted manuscript; J.E.H., O.E.J., and B.S.B. edited and revised manuscript; J.E.H., O.E.J., and B.S.B. approved final version of manuscript.

REFERENCES

1. **Ambrosi D, Pezzuto S.** Active stress vs. active strain in mechanobiology: constitutive issues. *J Elast* 107: 199–212, 2012.
2. **An SS, Bai TR, Bates JH, Black JL, Brown RH, Brusasco V, Chitano P, Deng L, Dowell M, Eidelman DH, Fabry B, Fairbank NJ, Ford LE, Fredberg JJ, Gerthoffer WT, Gilbert SH, Gosens R, Gunst SJ, Halayko AJ, Ingram RH, Irvin CG, James AL, Janssen LJ, King GG, Knight DA, Lauzon AM, Lakser OJ, Ludwig MS, Lutchen KR, Maksym GN, Martin JG, Mauad T, McParland BE, Mijailovich SM, Mitchell HW, Mitchell RW, Mitzner W, Murphy TM, Paré PD, Pellegrino R, Sanderson MJ, Schellenberg RR, Seow CY, Silveira PSP, Smith PG, Solway J, Stephens NL, Sterk PJ, Stewart AG, Tang DD, Tepper RS, Tran T, Wang L.** Airway smooth muscle dynamics: a common pathway of airway obstruction in asthma. *Eur Respir J* 29: 834–860, 2007.
3. **Bates JH, Bullimore SR, Politi AZ, Sneyd J, Anafi RC, Lauzon AM.** Transient oscillatory force-length behavior of activated airway smooth muscle. *Am J Physiol Lung Cell Mol Physiol* 297: L362–L372, 2009.
4. **Brook BS, Peel SE, Hall IP, Politi AZ, Sneyd J, Bai Y, Sanderson MJ, Jensen OE.** A biomechanical model of agonist-initiated contraction in the asthmatic airway. *Respir Physiol Neurobiol* 170: 44–58, 2010.

5. **Clifford PS, Ella SR, Stupica AJ, Nourian Z, Li M, Martinez-Lemus LA, Dora KA, Yang Y, Davis MJ, Pohl U, Meininger GA, Hill MA.** Spatial distribution and mechanical function of elastin in resistance arteries. *Arterioscler Thromb Vasc Biol* 31: 2889–2896, 2011.
6. **Fredberg JJ, Inouye D, Miller B, Nathan M, Jafari S, Raboudi SH, Butler JP, Shore SA.** Airway smooth muscle, tidal stretches, and dynamically determined contractile states. *Am J Respir Crit Care Med* 156: 1752–1759, 1997.
7. **Fredberg JJ, Inouye DS, Mijailovich SM, Butler JP.** Perturbed equilibrium of myosin binding in airway smooth muscle and its implications in bronchospasm. *Am J Respir Crit Care Med* 159: 959–967, 1999.
8. **Hai CM, Murphy RA.** Cross-bridge phosphorylation and regulation of latch state in smooth muscle. *Am J Physiol Cell Physiol* 254: C99–C106, 1988.
9. **Harvey BC, Parameswaran H, Lutchen KR.** Can tidal breathing with deep inspirations of intact airways create sustained bronchoprotection or bronchodilation? *J Appl Physiol* 115: 436–445, 2013.
10. **Hiorns JE, Jensen OE, Brook BS.** Nonlinear compliance modulates dynamic bronchoconstriction in a multiscale airway model. *Biophys J* 107: 3030–3042, 2014.
11. **Hoffman BD, Grashoff C, Schwartz MA.** Dynamic molecular processes mediate cellular mechanotransduction. *Nature* 475: 316–323, 2011.
12. **Holzapfel G, Gasser T, Ogden R.** A new constitutive framework for arterial wall mechanics and a comparative study of material models. *J Elast* 61: 1–48, 2000.
13. **Humphrey JD.** Remodeling of a collagenous tissue at fixed lengths. *J Biomech Eng* 121: 591–597, 1999.
14. **Humphrey JD, Dufresne ER, Schwartz MA.** Mechanotransduction and extracellular matrix homeostasis. *Nat Rev Mol Cell Biol* 15: 802–812, 2014.
15. **Huxley AF.** Muscle structure and theories of contraction. *Prog Biophys Biophys Chem* 7: 255–318, 1957.
16. **Isenberg B, DiMilla P, Walker M, Kim S, Wong J.** Vascular smooth muscle cell durotaxis depends on substrate stiffness gradient strength. *Biophys J* 97: 1313- 1322, 2009.
17. **Lambert RK, Paré PD.** Lung parenchymal shear modulus, airway wall remodeling, and bronchial hyperresponsiveness. *J Appl Physiol* 83: 140–147, 1997.
18. **Lambert RK, Wilson TA, Hyatt RE, Rodarte JR.** A computational model for expiratory flow. *J Appl Physiol* 52: 44–56, 1982.
19. **Lambert RK, Wiggs BR, Kuwano K, Hogg JC, Paré PD.** Functional significance of increased airway smooth muscle in asthma and COPD. *J Appl Physiol* 74: 2771–2781, 1993.
20. **Lan B, Deng L, Donovan GM, Chin LY, Syyong HT, Wang L, Zhang J, Pascoe CD, Norris BA, Liu JC, Swyngedouw NE, Banaem SM, Paré PD, Seow CY.** Force maintenance and myosin filament assembly regulated by Rho-kinase in airway smooth muscle. *Am J Physiol Lung Cell Mol Physiol* 308: L1–L10, 2015.
21. **LaPrad AS, Szabo TL, Suki B, Lutchen KR.** Tidal stretches do not modulate responsiveness of intact airways in vitro. *J Appl Physiol* 109: 295–304, 2010.
22. **Latourelle J, Fabry B, Fredberg JJ.** Dynamic equilibration of airway smooth muscle contraction during physiological loading. *J Appl Physiol* 92: 771–779, 2002.
23. **Lavoie TL, Krishnan R, Siegel HR, Maston ED, Fredberg JJ, Solway J, Dowell ML.** Dilatation of the constricted human airway by tidal expansion of lung parenchyma. *Am J Respir Crit Care Med* 186: 225–232, 2012.
24. **Lim TK, Pride NB, Inram JR.** Effects of volume history during spontaneous and acutely induced air-flow obstruction in asthma. *Am Rev Respir Dis* 135: 591–596, 1987.
25. **Lo CM, Wang HB, Dembo M, Wang YL.** Cell movement is guided by the rigidity of the substrate. *Biophys J* 79: 144–152, 2000.
26. **Macklem PT.** A theoretical analysis of the effect of airway smooth muscle load on airway narrowing. *Am J Respir Crit Care Med* 153: 83–89, 1996.
27. **Mijailovich SM, Butler JP, Fredberg JJ.** Perturbed equilibria of myosin binding in airway smooth muscle: Bond-length distributions, mechanics, and ATP metabolism. *Biophys J* 79: 2667–2681, 2000.
28. **Noble PB, Jones RL, Needi ET, Cairncross A, Mitchell HW, James AL, Mc- Fawn PK.** Responsiveness of the human airway in vitro during deep inspiration and tidal oscillation. *J Appl Physiol* 110: 1510–1518, 2011.
29. **Oliver MN, Fabry B, Marinkovic A, Mijailovich SM, Butler JP, Fredberg JJ.** Airway hyperresponsiveness, remodeling, and smooth muscle mass right answer, wrong reason? *Am J Respir Cell Mol Biol* 37: 264–272, 2007.
30. **Politi AZ, Donovan GM, Tawhai MH, Sanderson MJ, Lauzon AM, Bates JH, Sneyd J.** A multiscale, spatially distributed model of asthmatic airway hyperresponsiveness. *J Theor Biol* 266: 614–624, 2010.
31. **Taber LA, Humphrey JD.** Stress-modulated growth, residual stress, and vascular heterogeneity. *J Biomech Eng* 123: 528–535, 2001.
32. **Tse JR, Engler AJ.** Stiffness gradients mimicking in vivo tissue variation regulate mesenchymal stem cell fate. *PLoS One* 6.1: e15978, 2011.
33. **Wang I, Politi AZ, Tania N, Bai Y, Sanderson MJ, Sneyd J.** A mathematical model of airway and pulmonary arteriole smooth muscle. *Biophys J* 94: 2053–2064, 2008.
34. **Wang L, Paré PD, Seow CY.** Effects of length oscillation on the subsequent force development in swine tracheal smooth muscle. *J Appl Physiol* 88: 2246–2250, 2000.
35. **Watton PN, Hill NA, Heil M.** A mathematical model for the growth of the abdominal aortic aneurysm. *Biomech Model Mechanobiol* 3: 98–113, 2004.
36. **Wiggs BR, Hrousis CA, Drazen JM, Kamm RD.** On the mechanism of mucosal folding in normal and asthmatic airways. *J Appl Physiol* 83: 1814–1821, 1997.